ACS OMEGA

http://pubs.acs.org/journal/acsodf

Article

Metrology of Ar−N_2/O_2 Mixture Atmospheric Pressure Pulsed DC Jet Plasma and its Application in Bio-Decontamination

Naqib Ullah, Muhammad Ibrahim Khan, Anisa Qamar,* Najeeb-Ur Rehman,* ElSayed Tag elDin, Mohammad Alkhedher, and Abdul Majid

Cite This: *ACS Omega* 2023, 8, 12028−12038

Read Online

ACCESS | Metrics & More | Article Recommendations

ABSTRACT: Atmospheric pressure plasma jets are gaining a lot of attention due to their widespread applications in the field of bio-decontamination, polymer modification, material processing, deposition of thin film, and nanoparticle fabrication. Herein, we are reporting the disinfection of *Pseudomonas aeruginosa*, *Staphylococcus aureus*, and *Escherichia coli* bacteria using plasma jet. In this regard, Ar−O_2, Ar−N_2, and Ar−O_2−N_2 mixture plasma is generated and characterized using optical and electrical characterization. Variation in plasma parameters like electron temperature, electron density, and reactive species production is monitored with discharge parameters such as applied voltage and feed gas concentration. Results show that the peak average power consumed in Ar−O_2, Ar−N_2, and Ar−O_2−N_2 mixture plasma is found to be 4.45, 2.93, and 4.35 W respectively, at 8 kV. Moreover, it is noted that by increasing applied voltage, the electron temperature, electron density, and reactive species production also increases. It is worth noting that electron temperature increases with increase in oxygen concentration in the mixture (Ar − O_2), while it decreases with increase in nitrogen concentration in the mixture (Ar−N_2). Similarly, a decreasing trend in electron temperature is noted for Ar−O_2−N_2 mixture plasma. On the other hand, a decreasing trend in electron density is noted for all the mixtures. Reduction in viable colonies of *Pseudomonasaeruginosa*, *StaphylococcusAureus*, and *Escherichiacoli* were confirmed by the serial dilution method. The inactivation efficiency of pulsed DC plasma generated, in the Ar−N_2 mixture at 8 kV and 6 KHz, was evaluated against *P. aeruginosa*, *S. aureus* and *E. coli* bacteria by measuring the number of surviving cells versus plasma treatment time. Results showed that after 240 s of plasma treatment, the number of survival colonies of the mentioned bacteria was reduced to less than 30 CFU/mL.

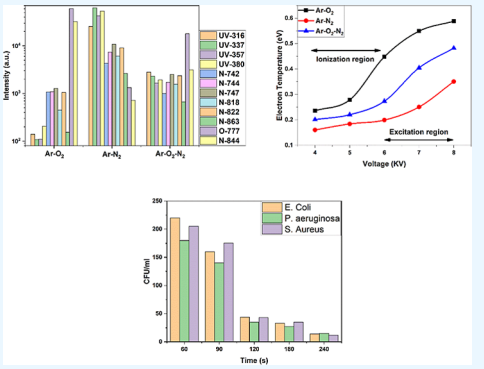

INTRODUCTION

Laboratory plasma has become a subject of great interest for a wide range of applications in various fields.[1−4] In industries, plasma is used in etching and synthesis of advanced materials,[5,6] synthesis of nanomaterials,[7,8] enhancement of electrical properties of semiconductor,[9] surface modification,[10] coating,[11] cleaning,[12] plasma-enhanced chemical vapor deposition of thin film solar cells,[13] processing of wastes,[14] water purification,[15] carbon dioxide dissociation and activation,[16] and so forth. Concerning medical application, plasma technologies are further divided into two categories:

1. Processing of surfaces, sterilization, and disinfection of bio-relevant instruments to achieve desired qualities for therapeutic purposes subsequently.
2. Direct interaction of plasma with human or animal organs for specific medical treatments.

Plasma-based treatments of medicinal instruments to modify their biocompatibility and to improve the polymer surfaces are largely studied to meet the criteria for cell culturing and tissue engineering.[17−19] Pioneer applications of plasma in medicinal field were sterilization and sanitization of medical equipment. Plasma technology showed brilliant results in sterilization, bacterial disinfection, and decontamination processes. The plasma-assisted disinfection techniques were made more advanced, and the field of dermatology was further explored.[20−22] Cold atmospheric pressure plasma has proven its anti-cancer effect in numerous in vitro and in vivo studies.[23] Similarly in dentistry, plasma research showed remarkable results in tooth whitening, removal of plaque, dental apparatus sterilization, bacterial disinfection, and in composite regeneration.[24]

Researchers throughout the globe are contributing to medical plasma.[25−32] However, physical and chemical impacts of plasma which play a vital role in medicine are still difficult to understand. Moreover, the bio-relevant targets which are used

Received: December 7, 2022
Accepted: March 2, 2023
Published: March 23, 2023

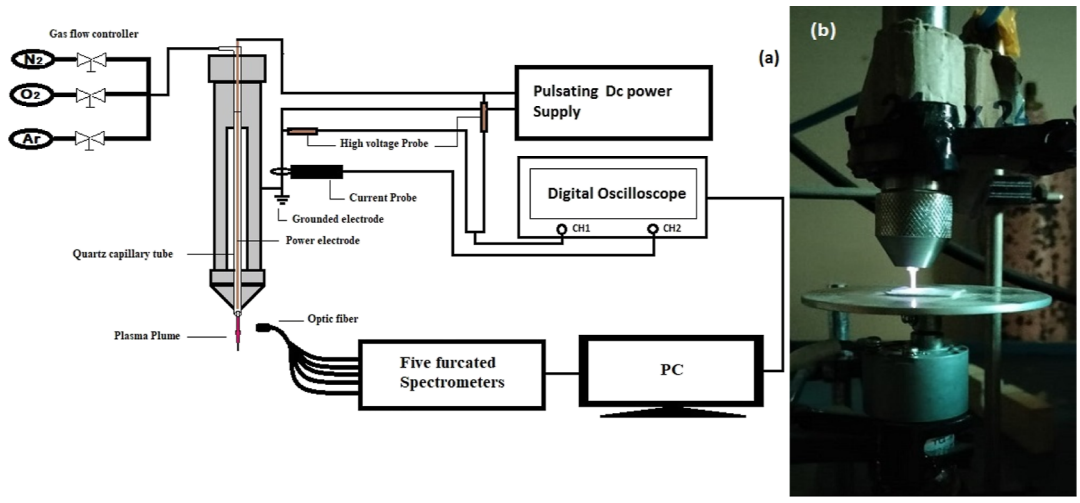

Figure 1. (a) Schematic diagram of the experimental setup; (b) real-time discharge in developed KINPen (photograph courtesy of "Naqib Ullah". Copyright 2023).

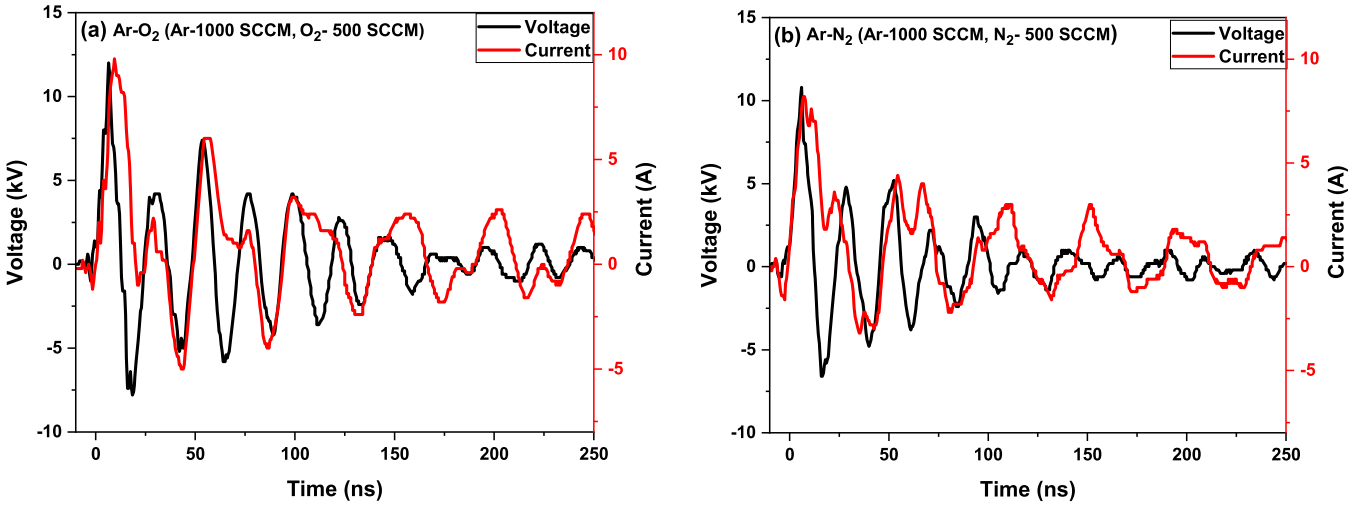

Figure 2. Current−voltage waveform of discharge at 8 kV voltage and 6 kHz fixed pulsed frequency in (a) Ar−O_2 and (b) Ar−N_2 mixture plasmas.

in treatment are quite complex due to various unmeasured and mysterious variables.[33−35] However, atmospheric pressure plasma comprises of reactive nitrogen and oxygen species (RNOS), having gas temperature close to ambient temperature, and is suitable for biomedical applications.[36−41] In addition to RNOS, UV radiation and transient electric fields are also likely important in plasma-based disinfection.[42−47] Tuning of these parameters at ambient temperature is always a challenge due to high electron neutral collision rates. Numerous atmospheric pressure devices have been developed to generate the room temperature plasma for medical and industrial applications.[48−53] Investigation on plasma devices emphasizing on biomedical applications has shown that plasma devices can be economical and convenient.[54] In these devices, discharge parameters influence the biological sample, which can be controlled via plasma parameters like input power, treatment time, treatment distance, feed gas composition, and mode of operation.[55]

The primary objective of the present study is to optimize plasma parameters, that is, electron number density, electron temperature, and power consumed in terms of discharge parameters, that is, applied voltage and gases concentrations, for inactivation of different pathogenic bacteria (*Pseudomonas Aeruginosa*, *StaphylococcusAureus*, and *Escherichiacoli*). To study the effect of molecular gases concentrations on plasma parameters, the total flow rate (1500 SCCM) of the mixture is kept constant, while the molecular gas content is varied as follows: in Ar−O_2 plasma, the O_2 concentration is varied from 5 to 50% of the total flow rate; in Ar−N_2 plasma, the N_2 concentration is varied from 5 to 50% of the total flow rate; and in Ar−O_2−N_2 plasma, the O_2 and N_2 have equal flow rates; the O_2 + N_2 concentration is varied from 5 to 50% of the total flow rate.

To understand the kinetics of the discharge, optical emission spectroscopy (OES) and electrical characterization techniques are employed. Electron density is estimated by using physical−electrical and Stark broadening techniques. Average power consumed per pulse is calculated from electrical measurements. Normalized intensities of RNOSs, UV radiation, and electron temperature are monitored as function of discharge parameters.

EXPERIMENTAL SETUP

The schematic diagram of experimental setup is shown in Figure 1. A home-made cylindrical plasma jet with the source

https://doi.org/10.1021/acsomega.2c07810
ACS Omega 2023, 8, 12028−12038

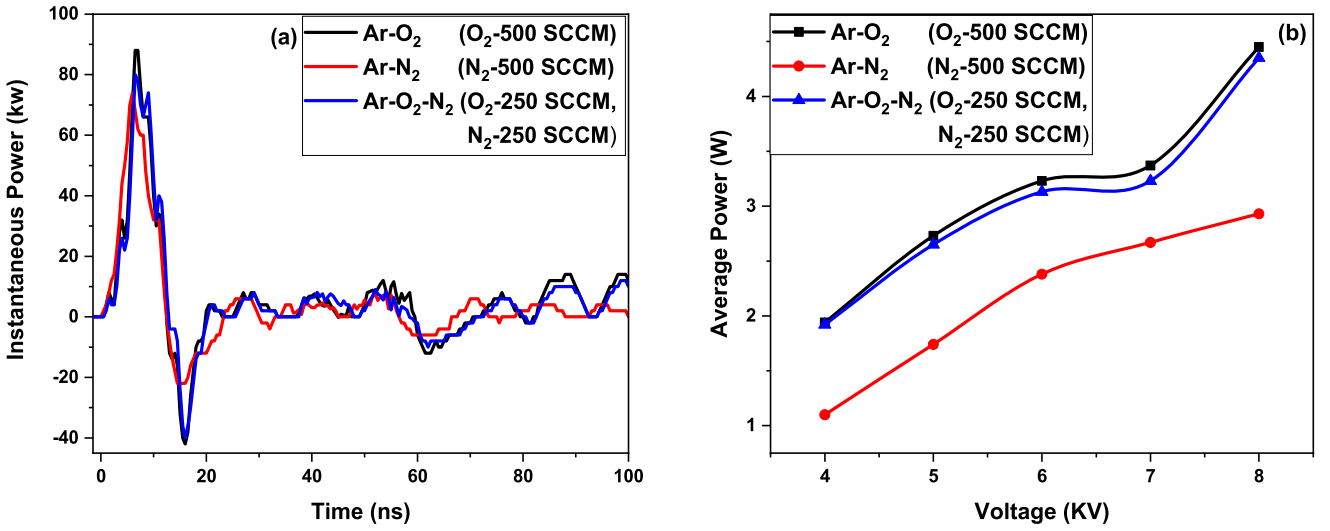

Figure 3. Evolution of (a) instantaneous discharge power at 8 KV and (b) average discharge power verses applied voltage in Ar−O_2, Ar−N_2, and Ar−O_2−N_2 mixture plasma, recorded at 6 kHz frequency and 1500 SCCM total gas flow rate.

tube of length 90 mm, operating at atmospheric pressure was used to generate the plasma. The outer body of the source tube, served as the cathode, was made of stainless-steel of diameter 16 mm, while the inner diameter was 12 mm. To make it electrical safe, a Teflon rod, of outer diameter 12 mm, was inserted in the stainless-steel pipe. For dielectric barrier discharge (DBD) configuration a quartz tube of outer diameter 4 mm and inner diameter 2 mm was fixed in the Teflon rod. A copper wire, serving as the anode, was inserted through this quartz tube. To generate the plasma, a nanosecond pulse DC power supply (FPG10-10NM10) was used, at a fixed frequency of 6 kHz while the applied voltage was varied from 4 to 8 kV with a step of 1 kV. To monitor the effect of gases' flow rate on plasma parameters, it was varied up to 1500 SCCM with Teledyne digital mass flowmeters.

OES was employed to record the time-integrated emission spectra as a function of discharge parameters. The emission spectra of the discharge were recorded using a set of collimated lens and optic fiber (FC5-UV/IR200-2-ME), positioned at the right angle to the discharge, and connected to high resolution spectrometer (AVANTES-RACKMOUNT-USB2). These five furcated spectrometers were equipped with five gratings with a bandwidth of 250−900 nm. The first two gratings have 2400 lines/mm, next two have 1800 lines/mm, and the last one has 1200 lines/mm. The respective resolution varies from 0.06 to 0.13 nm. The TOSHIBACCD (Linear array 3648DUV) detector of 8 μm pitch was installed in the spectrometer. A high voltage probe (TESTECTT-HVP2739) with a bandwidth of DC-220 MHz and the current probe (GwINSTEKGCP-530) with a bandwidth of DC-50 MHz were used to monitor the voltage and current characteristics of the discharge. To avoid the reflection effect, on recorded traces, a suitably long transmission line was used. Moreover, to measure the net applied voltage of the discharge, measurements were carried out very close to the electrodes.

RESULTS AND DISCUSSION

Electrical Characterization of the Discharge. Figure 2 shows the recorded voltage and current waveforms of discharge, in plasma jet, as a function of time, for (a) Ar−O_2 (Ar 1000 SCCM, O 2500 SCCM) and (b) Ar−N_2 (Ar-1000 SCCM and N2-500 SCCM) mixture plasma, at 8 kV applied voltage and 6 kHz fixed frequency.

A GWInstek3000 series four channel oscilloscope (GDS-3504), having 500 MHz bandwidth and 4 Gsample/second real time sampling rate, was used to record waveforms for each pulse of voltage and corresponding discharge current. The pulsating DC power supply has a rise time of 2−3 ns and uses a square wave of pulse width 10 ns and 50% duty cycle as the input signal to initiate the discharge, but the output signals from the load collected via an oscilloscope were quite different. This may be referred to as the mismatch of impedance between load (discharge) and power supply, which results in multiple harmonics of the applied signal inside the plasma. The repetitive voltage and current signals confirm that the pulsed supply is well adapted to the charge setup. The influence of electromagnetic perturbations on the shape of pulse waveforms and the reflection of power back to cable are also visible (Figure 2) in terms of some kV amplitudes, which appear after 20 ns, but these perturbations are not influencing adequately the discharge performance. It is clear from the figure that the current waveforms are in phase with the voltage waveforms peaks. The positive current peaks at the rising and falling ends of the voltage peak are formed due to the propagation of charges from the power electrode to the surface of the dielectric barrier within the plasma. The dropping regime of current appears when pulse voltage starts to decrease from its highest amplitude to zero. These negative peaks of current appear when the charges are collected back by the power electrode.

Power Consumed. By using these IV curves, the average discharge powers can be calculated by taking area under the curve using eq 1.

$$P_{ave} = \frac{1}{T}\int_0^t V(t)I(t)\mathrm{d}t \quad (1)$$

where T is the time period of applied frequency, and $V(t)$ and $I(t)$ are the voltage and current traces recorded using voltage and current probes respectively. For estimation of average power, the recorded $V(t)$ and $I(t)$ traces were integrated for pulse duration of 20 ns. The term power here refers only to the

https://doi.org/10.1021/acsomega.2c07810
ACS Omega 2023, 8, 12028−12038

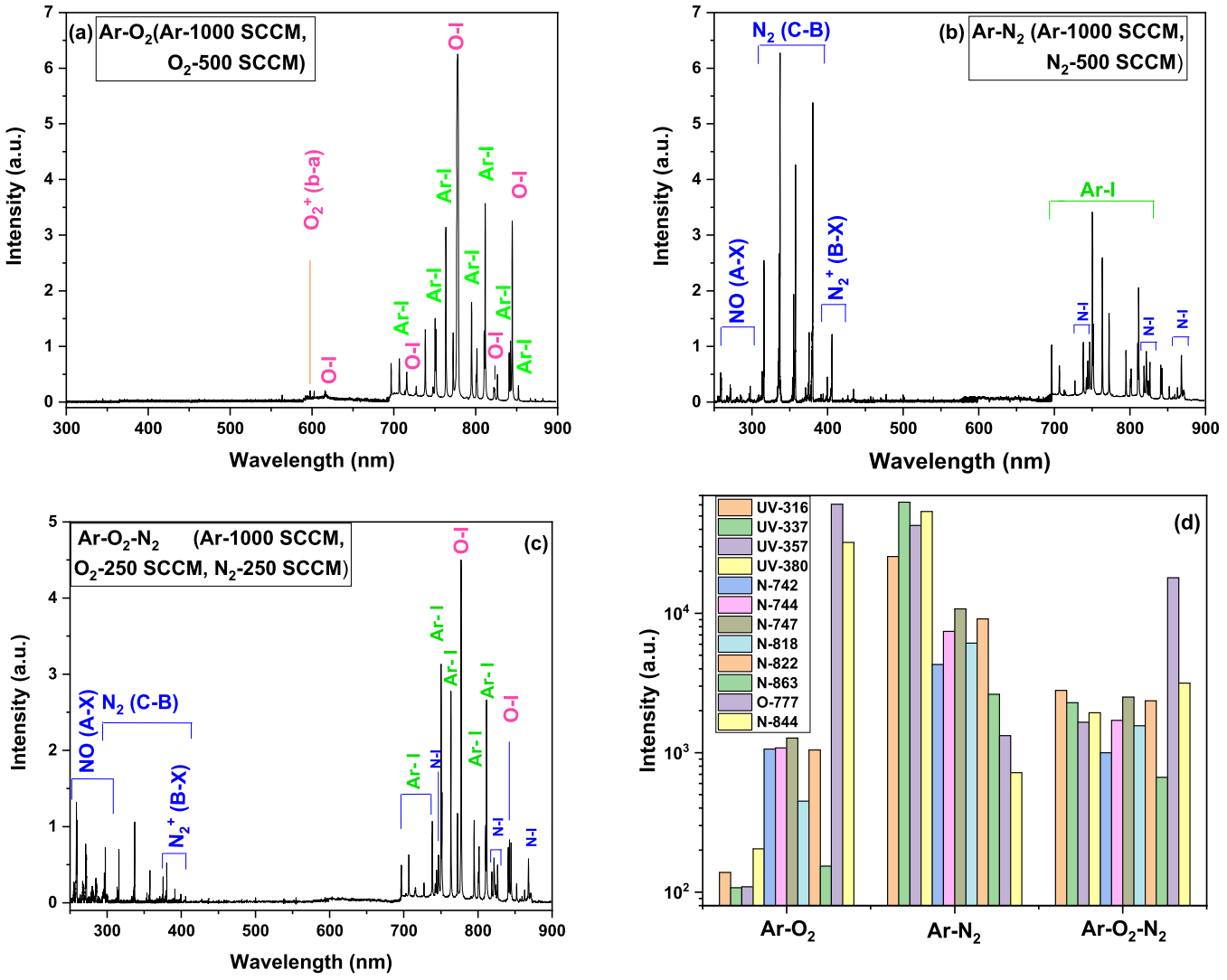

Figure 4. Optical emission spectra of (a) Ar−O_2, (b) Ar−N_2, (c) Ar−O_2−N_2, and (d) normalized intensities of UV radiation, reactive nitrogen, and oxygen species, recorded at 8 kV applied voltage, 6 kHz fixed frequency, and 1500 SCCM flow rate.

power consumed, which is obtained as a product of energy per pulse (Joules) and supply frequency (kHz).

Different maximum instantaneous powers (Figure 3a), for example, 88, 74, and 80 kW are measured for Ar−O_2, Ar−N_2, and Ar−O_2−N_2 mixtures, respectively, for a fixed applied voltage of 8 kV. The area under the curve of these instantaneous power versus time graphs gives the energy consumed per pulse in Joules for a particular combination of supply voltage and frequency. This energy per pulse is multiplied by the supply frequency to obtain the average power consumed by the device in Watt (W). The maximum average power consumed in Ar−O_2, Ar−N_2, and Ar−N_2−O_2 mixtures discharges are 4.45, 2.93, and 4.35 W, respectively, at 8 kV applied voltage (Figure 3b) under the similar discharge conditions. It is clear from Figure 3b that the Ar−O_2 mixture consumes large average power compared to Ar−N_2 and Ar−O_2−N_2 mixtures. The difference in power consumed by the device when different working gasses are used is due to the various ionization mechanisms of different gases. In Ar−O_2 plasma, due to the high electron affinity of oxygen, the plasma resistance increased and require more power to sustain the discharge as compared to Ar−N_2 plasma. Furthermore, the oxygen gas is electronegative in nature and the loss of electrons due to diffusion and attachment to oxygen molecules in Ar−O_2 plasma requires high electric field strength inside the plasma than Ar−N_2 plasma to produce enough electrons to sustain the discharge.

Optical Emission Spectroscopy. *Identification of Spectra.* In non-thermal plasmas, the ion temperature is almost equal to room temperature, whereas the electron temperature is around a few thousand kelvin. These energetic electrons are responsible for plasma generation via electron impact excitation and ionization. Besides this, these energetic electrons play a crucial role in the generation of reactive species by dissociating the molecules into atoms. RNOs, nitrogen oxides (N_xO_y), hydroxyl radicals (OH), ozone (O_3), and molecular ions can be formed by electron impact.[56−58]

In the present study, OES was carried out to understand the ongoing process in the generated plasma. The emission spectra of Ar − O_2(Ar − 1000 SCCM and O_2 − 500 SCCM), Ar − N_2(Ar − 1000 SCCM and N_2 − 500 SCCM) and Ar − O_2 − N_2(Ar − 1000 SCCM, O_2 − 250 SCCM and N_2 − 250 SCCM) gases mixtures, in the active plasma region, recorded at 8 kV

https://doi.org/10.1021/acsomega.2c07810
ACS Omega 2023, 8, 12028−12038

applied voltage, 6 kHz frequency and 1500 SCCM total gas flow rate, are shown in Figure 4.

In Ar−O_2 plasma discharge, highly reactive atomic oxygen species comprising of (a) $3s^3S-3p^3P$ around 844.6 nm, (b) $3s^3D-3p^3D$ around 823.3 nm, (c) $3s^5S-3p^5P$ around 777.4 nm, (d) $3s^1D-3p^3P$ around 715.7 nm, and (e) $3p^5P-4d^5D$ around 615.8 nm along with Ar−I and Ar−II lines are detected. The first negative system of O_2 molecule O_2^+ ($b^4\Sigma_g^- - a^4\Pi_u$)[59] in the spectral range of 596−609 nm is shown in Figure 4a. It is worth noting that the probability of dissociation of O_2 through collision with electrons is quite low because O_2 has a high electronegative nature.[60] The one possible reaction is that the energetic electrons first excite the Ar atoms to some highly excited metastable state which, through collisions with O_2 molecules, transfer energy to O_2 molecules to either dissociate or even ionize them to O_2^+. The second possibility is that the Ar atoms transfer their energy to O_2 molecules and O_2 molecules become super excited. This super excited molecule can dissociate into O* and O as

$$e^* + Ar \rightarrow Ar^* + e \quad (2)$$

$$Ar^* + O_2 \rightarrow O_2^{**} + Ar \quad (3)$$

$$O_2^{**} \rightarrow O^* + O \quad (4)$$

Alternatively, super excited molecules could first autoionize to form an O_2^+ ion; then the O_2^+ ion captures an electron and dissociates into O atoms as reported in literature[61]

$$O_2^{**} \rightarrow O_2^+ + e \quad (5)$$

$$e + O_2^+ \rightarrow O + O \quad (6)$$

$$e + O_2^+ \rightarrow O^+ + O + e \quad (7)$$

Figure 4b shows the normalized emission intensities in Ar−N_2 mixture plasma; 16 different multiplets of N atoms: (a) 3 transitions at 742.3, 744.2, and 746.8 nm associated with $3s^4P-3p^4S$, (b) 5 transitions at 818.5, 820, 821.6, 822.3, and 824.2 nm associated with $3s^4P-3p^4P$, (c) 4 transitions at 856.8, 859.4, 862.9, and 856.6 nm associated with $3s^2P-3p^2P$, and (d) 4 transitions at 868, 870.3, 871.2, and 871.9 nm associated with $3s^4P-3p^4D$ are observed. The emission spectra in the UV region composed of the NO band at (258.6 nm), with electronic transition ($NO(A^2\Sigma^+ - X^2\Pi_r)$), N_2 second positive system at (315−380 nm), with electronic transition ($N_2(C^3\pi_u - B^3\pi_g)$), and N_2 first negative system at N_2^+(391−428 nm) with electronic transition (N_2^+ ($B^2\Sigma_u - X^2\Sigma_g$)) are clearly visible in Figure 4b.

These predominant bands of NO, N_2 ($C^3\Pi_u$), and N_2^+ ($B^2\ \Sigma_u^+$) are excited as[62,63]

$$NO(X^2\Pi) + N_2(A^3\Sigma_u^2) \rightarrow N_2(X^2\Sigma_g) + NO(A^2\Sigma^+) \quad (8)$$

$$NO(A^2\Sigma^+) \rightarrow NO(X^2\Pi) + h\nu \quad (9)$$

$$N_2(X^1\Sigma_g^+) + e^* \rightarrow N_2(C^3\Pi_u) + e \quad (10)$$

$$N_2(X^1\Sigma_g^+) + Ar^*(^3P_2, {}^3P_2) \rightarrow N_2(C^3\Pi_u) + Ar \quad (11)$$

$$N_2(X^1\Sigma_g^+) + e \rightarrow N_2^+(B^2\ \Sigma_u^+) + 2e \quad (12)$$

Further, OES analysis revealed that Ar peaks are more dominant over other species such as oxygen and nitrogen. Since a higher flow of argon was introduced in the APPJ device, the bright purple color can be attributed to this dominant species.

(1) The transition involving singlet, triplet, and quintet levels is observed.
(2) The transition between quintet levels of oxygen is higher than the transition between triplet levels.

The normalized intensities of UV radiation and reactive species plotted (on log scale graph) for a fixed applied voltage of 8 kV in different Ar−O_2, Ar−N_2, and Ar−N_2−O_2 mixture plasma are shown in Figure 4d. It is clear from the figure that in Ar−O_2 plasma, the UV radiation is negligible; the reactive nitrogen species intensities are moderate while reactive oxygen species intensities are high. However, in Ar−N_2 mixture plasma, the intensities of UV radiation and reactive nitrogen species are considerably high and also the reactive oxygen species intensities are moderate. For Ar−O_2−N_2 mixture plasma, the intensities of UV radiation and RNOs lie in between the Ar−O_2 and Ar−N_2 plasma. Since the concentrations of UV radiation and RNOs are more appropriate for plasma-based disinfection, Ar−N_2 mixture plasma is employed for selected bacterial inactivation in this study.[64]

Electron Temperature. To control the production and destruction rates of reactive species in a plasma, accurate knowledge about the electron temperature is mandatory because these rates are the function of electron temperature. In the present study, electron temperature is estimated via the Boltzmann plot method based on the OES technique.[65] In this method, different lines of Ar−I are selected by assuming that these lines are populated according to Boltzmann distributions.[66] Table 1 shows the selected Ar−I lines used to estimate the electron temperature, whereas the relevant spectroscopic data are taken from literature.[67] The transitions from Ar−I lines used to calculate the electron temperature are given in Table 1.

Table 1. Spectroscopic Data of Ar−I Transition Used in the Boltzmann Plot for Electron Temperature Measurement

wavelength (nm)	$A_k(10^6\ S^{-1})$	g_k	E_k (eV)
727.29	1.83	3	13.32
738.39	08.5	5	13.30
750.38	45.0	1	13.48
751.40	40.0	1	13.27
763.51	24.5	5	13.17
772.42	11.7	3	13.33
794.82	18.6	3	13.28
800.61	04.9	5	13.17
801.47	09.3	5	13.09
810.37	25.0	3	13.15
811.53	33.0	7	13.07
826.45	15.3	3	13.32
840.82	22.3	5	13.30
842.46	21.5	5	13.09

The dependency of electron temperature on applied voltage in Ar−O_2, Ar−N_2, and Ar−N_2−O_2 mixture plasma is plotted in Figure 5a. An increasing trend in electron temperature is noted with increasing applied voltage, which is because the power consumption increases with increasing applied voltage.

https://doi.org/10.1021/acsomega.2c07810
ACS Omega 2023, 8, 12028−12038

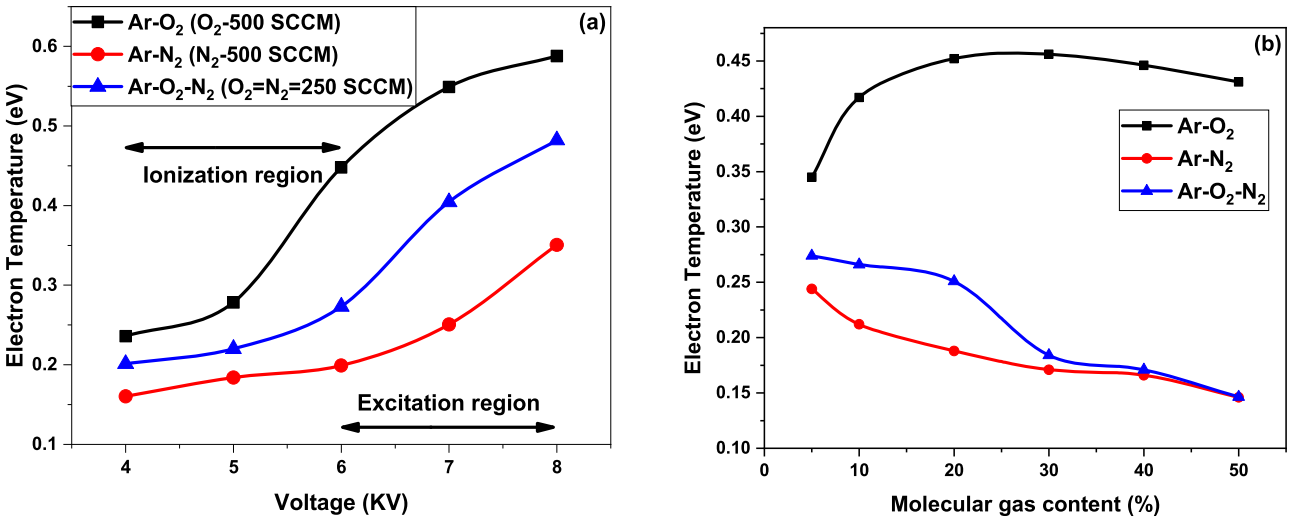

Figure 5. Variations of electron temperature (at 8 kV applied voltage, 6 kHz fixed frequency, and 1500 SCCM gas flow) vs (a) applied voltages and (b) molecular gas concentration.

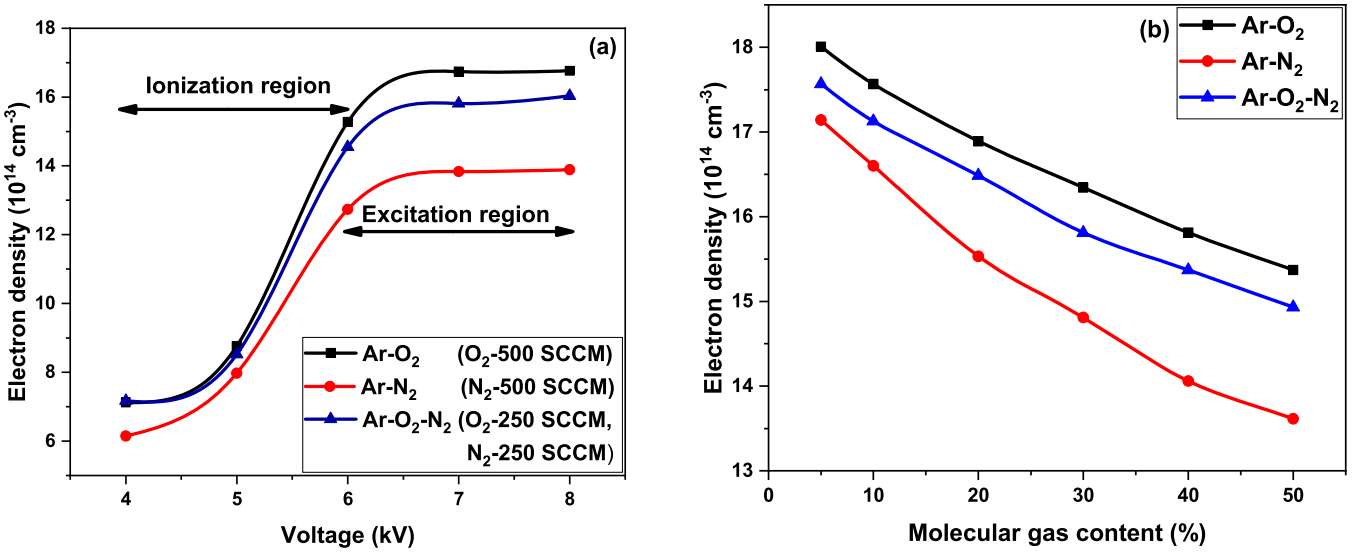

Figure 6. Variations of electron number density (at 8 kV applied voltage, 6 kHz fixed frequency, and 1500 SCCM flow rate) vs (a) applied voltages and (b) molecular gas concentration.

Furthermore, electron temperature has higher value in Ar−O_2 plasma as compared to Ar−N_2 plasma and Ar−O_2−N_2 plasma because Ar−O_2 plasma consumes more power than the remaining two types of plasmas, as shown in Figure 3b.

The electron temperature versus varying molecular gas concentrations is plotted in Figure 5b. In the case of Ar−O_2 plasma, increasing O_2 concentration results in increasing electron temperature, which may be due to the fact that increasing O_2 concentration reduces plasma excitation, especially in the UV region, so the consumed power is utilized to enhance the electron temperature.[68] In the case of Ar−N_2 and Ar−O_2−N_2 plasma, the decreasing trend in electron temperature is observed with increasing nitrogen concentration, which is because introducing nitrogen to argon plasma enhances the excitation and ionization in the UV region (Figure 4).[69] These enhanced excitations and ionization in the UV region, with the increasing N_2 concentration in the mixture, are due to higher electron impact cross section of nitrogen.[65] Hence, with the addition of nitrogen in the mixture, lower electron temperature is noted. Moreover, Penning excitation of the N_2 second positive system of nitrogen with a Ar metastable state also becomes predominant, and thus, a decrease in electron temperature is noted.[70]

Electron Number Density. In several dielectric media, the electrical phenomena are mostly related with the development and propagation of ionization waves. These waves play a vital role in the pre-breakdown processes and can be seen in a variety of pulsed electrical discharges like, DBD, coronal discharge, and lightning flashes.[71,72] Cold atmospheric pressure plasma jets have recently been discovered to exhibit similar phenomena associated to the rapid propagation of plasma luminous particles (plasma bullets/streamers).[73−75] In these discharges, plasma excitation is due to ionization wave propagation where space charge electric field plays a key role. To measure this electric field, one needs to solve the Boltzmann equation when plasma approximation is not valid. However, at low frequency (used in this study), one can measure the electric field using Laplacian ($E = -\nabla v/\nabla r$) as a

https://doi.org/10.1021/acsomega.2c07810
ACS Omega 2023, 8, 12028−12038

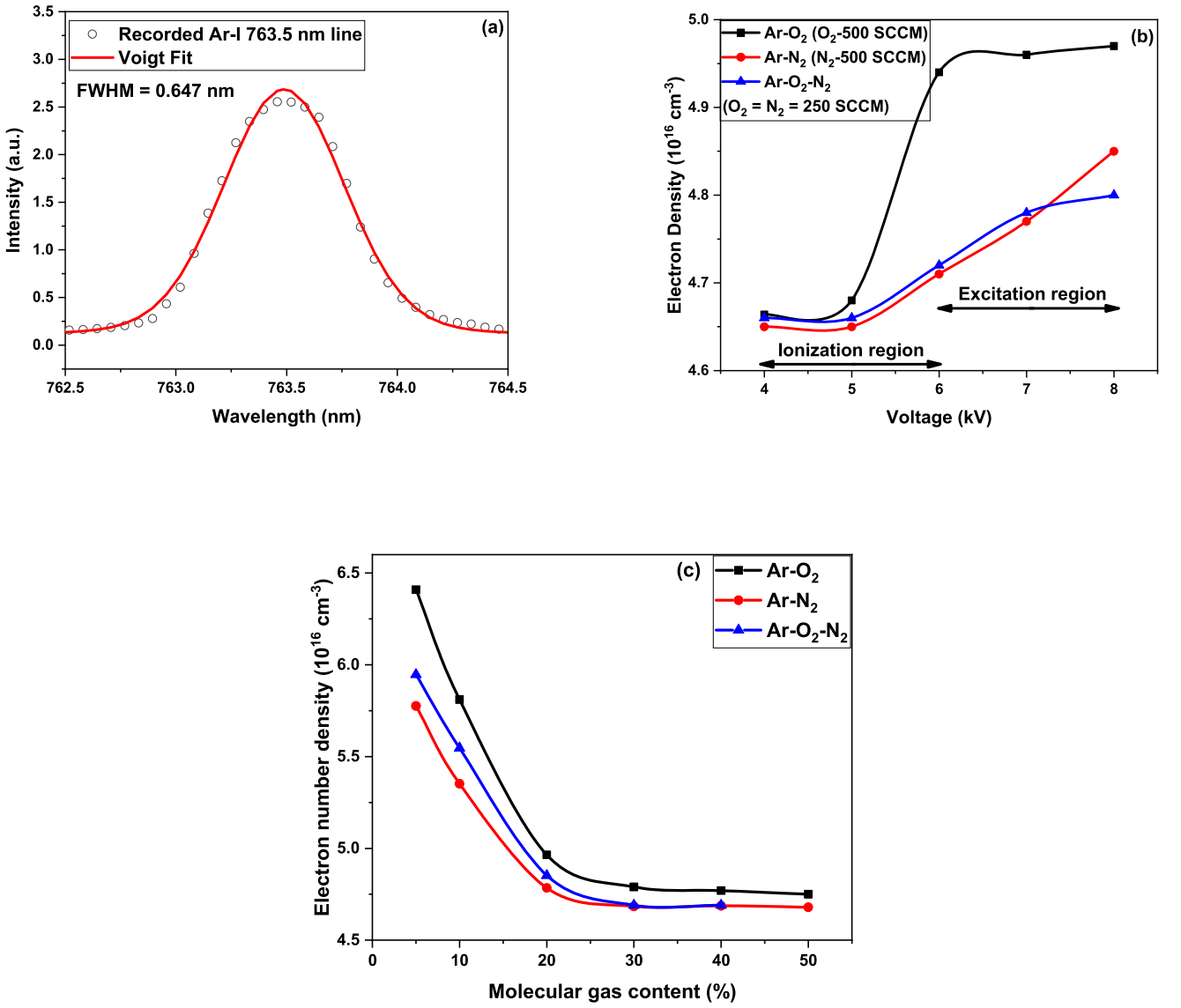

Figure 7. (a) Recorded Ar−I 763.5 nm line and Voigt Fit, (b) electron density vs applied voltage, and (c) electron density vs molecular gas concentration (at 8 kV applied voltage, 6 kHz fixed frequency, and 1500 SCCM total gas flow).

first approximation. The same is used to estimate the electron density using physical electrical measurement as

$$N_e = \frac{J}{\mu_e eE} \tag{13}$$

where N_e is electron number density, J is current density, μ_e is the mobility of electrons, e is a charge on the electron, and E is the electric field.[76] The variation of electron number density with different applied voltages and molecular gas content is shown in Figure 6.

It is clear from Figure 6 that the number density increases with an increase in applied voltage and decreases with increasing molecular gas concentration. This is because, at the higher applied voltage, the discharge current increases due to higher intensity of electric fields. As a result, the ionization rate of neutral species increases, which in turn is responsible for the increase in electron number density. Moreover, with increasing molecular gas concentration in the plasma, the energy transformation from electrons to molecules through vibrational and rotational excitations becomes more pronounced.[77] As a result, electron impact ionization decreases, as shown in Figure 6b. Further, the electron density in Ar−O_2 mixture plasma is higher than that of the Ar−N_2 and Ar−O_2−N_2 gaseous mixture plasmas. This is because the ionization energy of N_2 molecule is higher compared to the O_2 molecule.

Electromagnetic perturbations can influence the shape of pulse waveforms and may cause the inconsistency in the physical electrical measurement of electron number density. To overcome these limitations and for the sake of comparison, the electron number density is also measured with the "Stark broadening Technique" based on the OES. The Stark broadening mechanism is commonly used to measure the electron number density from the spectral line and is considered a significant non-intrusive plasma diagnostic technique.[78] In the absence of hydrogen lines, the neutral lines exhibit the quadratic Stark effect, and the relationship between electron number density and Stark broadening is given as.[79,80]

https://doi.org/10.1021/acsomega.2c07810
ACS Omega 2023, 8, 12028−12038

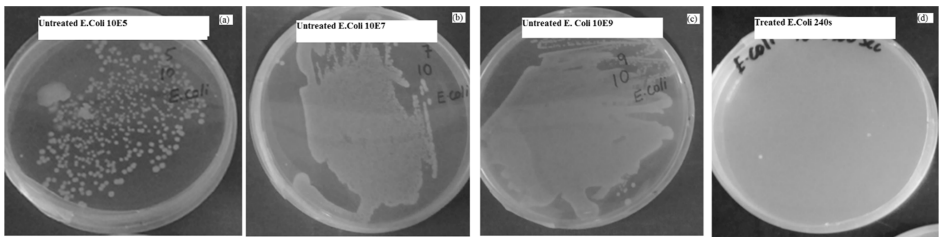

Figure 8. Growth of *E. coli* (a) 10^5 CFU/mL, (b) 10^7 CFU/mL, (c) 10^9 CFU/mL, and (d) treated for 240 s (photograph courtesy of "Naqib Ullah". Copyright 2023).

$$\Delta\lambda_{1/2} = 2\omega\left(\frac{N_e}{10^{16}}\right) + 3.5A\left(\frac{N_e}{10^{16}}\right)^{1/4}\left[1 - \frac{3}{4}N_D^{-1/3}\right] \omega\left(\frac{N_e}{10^{16}}\right) \quad (14)$$

where ω represents the electron impact width parameter, N_e denotes electron number density, A is the ion broadening parameter, and N_D is the number density of the Debye sphere. The first term of the abovementioned equation is due to electron's impact on broadening, while the second term is due to the ion's impact. In dense plasma, the non-hydrogenic isolated neutral atom is broadened by electron's impact, then the expression becomes

$$\Delta\lambda_{1/2} = 2\omega\left(\frac{N_e}{10^{16}}\right) \quad (15)$$

Numerous Ar I lines have been identified in the spectrum. The Ar I line at the 763.5 nm line is well evident, isolated, and also sensitive to the quadratic Stark effect and thus selected for electron density measurements based on OES.[77] Figure 7a shows the Voigt profile of the selected Ar I line. The value fwhm of the profile gives the Stark broadening, whereas the value of ω for Ar I 763.5 nm line is taken from literature.[77]

It is evident from the figure that the electron density measured via Stark broadening (eq 15) has one order value (10^{16} cm^{-3}) as compared to density measured via electrical measurement (eq 13). The trend for density versus molecular gas content is similar as electrical measurements. It is worth noting that from 4 to 6 kV, the electron density increases rapidly, but the electron temperature is almost constant, while from 6 to 8 kV, the electron density is almost constant, but the electron temperature increases.

Bacterial Inactivation. To check the efficiency of Ar−N_2 mixture plasma in sterilization of pathogenic bacteria, preferred suitable condition, that is, (Ar1000 SCCM − $N_2$500 SCCM) at 8 kV and 6 kHz frequency, for various exposure time was tested. For this purpose, three different bacteria (*Pseudomonas aeruginosa*, *Staphylococcus aureus*, and *Escherichia coli*) were selected. A bacterial suspension was prepared for *P. aeruginosa* bacteria with specific concentrations. 0.1 mL of an overnight broth of *P. aeruginosa* was taken (roughly containing 10^9 CFU/mL, CFU stands for colony forming units) from the prepared solution and evenly spread over the Petri dish. The Petri dish was placed on a DC gear motor to rotate under the plasma jet so that a larger area may interact with the plasma plume and each segment of the sample be uniformly treated. The serial dilution method was employed to dilute to the desired number of colonies and also for counting the viable colonies before and after plasma treatment. A similar procedure was repeated for *S. aureus* and *E. coli*. Each experiment was repeated at least three times, and the standard deviations are calculated. The growth of *E.coli* for various concentrations and after plasma treatment is shown in Figure 8.

Primary tests of the Ar−N_2 mixture plasma jet sterilization of pathogenic bacteria were executed to evaluate the effect of plasma sterilization of bacteria resistant to antibiotics. In the first step, the efficacy was checked for different motor speeds (0.5−50 rpm). It was found that the number of survival colonies was less with a 6 rpm speed. The number of survival colonies at different treatment times is shown in Figure 9. It is clear from the figure that the selected pathogenic bacteria deactivated with plasma treatment and exposure time. After 240 s, the number of survival colonies is reduced to less than 30.

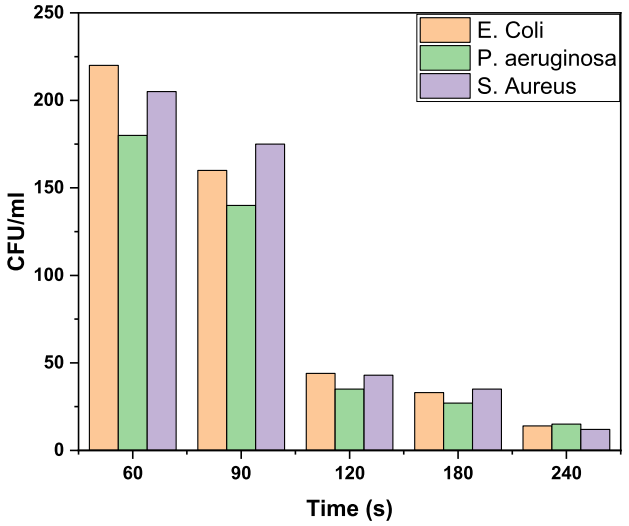

Figure 9. Number of survival colonies after Ar−N_2 (Ar-1000 SCCM and N_2-500 SCCM) plasma treatment at 8 kV voltage and 6 kHz frequency.

CONCLUSIONS

Electrical and optical characterization of Ar−O_2, Ar−N_2, and Ar−O_2−N_2 mixture plasma was carried out. The average power consumed was estimated at 4.45, 2.93, and 4.35 W, respectively. The emission spectrum reveals that in Ar−O_2 plasma, the UV radiation is negligible; normalized reactive nitrogen intensities are moderate, while normalized reactive oxygen species intensities are high. However, in Ar−N_2 mixture plasma, the normalized intensities of UV radiation and reactive nitrogen species are considerably high; also, the normalized reactive oxygen species intensities are moderate. For Ar−O_2−N_2 mixture plasma, the normalized intensities of UV radiation and RNOs lie in between the Ar−O_2 and Ar−N_2

https://doi.org/10.1021/acsomega.2c07810
ACS Omega 2023, 8, 12028−12038

plasma. Electron temperature increases with increasing voltage and increasing oxygen concentration in the mixture. On the other hand, increasing nitrogen concentration in the mixture causes a decrease in electron temperature. The electron density calculated from physical electrical technique shows an increasing trend with applied voltage, but a decreasing trend is noted by increasing molecular gas content. A similar trend was observed by estimating electron density via the OES-Stark broadening method. The electron density ($10^{14} - 10^{15}$) estimated from physical electrical technique is one order less than the electron density (10^{16}) derived from OES-Stark broadening mechanism. The deactivation of *P. aeruginosa*, *S. aureus*, and *E. coli* was reported with the application of $Ar-N_2$ mixture plasma.

AUTHOR INFORMATION

Corresponding Authors

Anisa Qamar − *Department of Physics, University of Peshawar, Peshawar, Khyber Pakhtunkhwa 25120, Pakistan*; Email: anisaqamar@uop.edu.pk

Najeeb-Ur Rehman − *Plasma Research Lab. Department of Physics, COMSATS University, Islamabad 45550, Pakistan*; orcid.org/0000-0001-6062-5836; Email: najeeb-ur-rehman@comsats.edu.pk

Authors

Naqib Ullah − *Department of Physics, University of Peshawar, Peshawar, Khyber Pakhtunkhwa 25120, Pakistan; Plasma Research Lab. Department of Physics, COMSATS University, Islamabad 45550, Pakistan*; orcid.org/0000-0002-2207-7848

Muhammad Ibrahim Khan − *Department of Physics, University of Science & Technology, Bannu, Khyber Pakhtunkhwa 28100, Pakistan*; orcid.org/0000-0002-5734-3667

ElSayed Tag elDin − *Electrical Engineering Department, Faculty of Engineering & Technology, Future University in Egypt, New Cairo 11835, Egypt*

Mohammad Alkhedher − *Mechanical and Industrial Engineering Department, Abu Dhabi University, Abu Dhabi 111188, United Arab Emirates*

Abdul Majid − *Department of Physics, University of Gujrat, Gujrat 50700, Pakistan*

Complete contact information is available at: https://pubs.acs.org/10.1021/acsomega.2c07810

Notes

The authors declare no competing financial interest.

ACKNOWLEDGMENTS

This work was supported by HEC Pakistan under NRPU project #9740 and TDF-137.

REFERENCES

(1) Lu, X.; Liu, D.; Xian, Y.; Nie, L.; Cao, Y.; He, G. Cold atmospheric-pressure air plasma jet: Physics and opportunities. *Phys. Plasmas* **2021**, *28*, 100501.

(2) Mir, S. A.; Shah, M. A.; Mir, M. M. Understanding the role of plasma technology in food industry. *Food Bioprocess Technol.* **2016**, *9*, 734−750.

(3) Attri, P.; Ishikawa, K.; Okumura, T.; Koga, K.; Shiratani, M. Plasma agriculture from laboratory to farm: A review. *Processes* **2020**, *8*, 1002.

(4) Laroussi, M. Cold plasma in medicine and healthcare: The new frontier in low temperature plasma applications. *Front. Phys.* **2020**, *8*, 74.

(5) Oehrlein, G. S.; Hamaguchi, S. Foundations of low-temperature plasma enhanced materials synthesis and etching. *Plasma Sources Sci.* **2018**, *27*, 023001.

(6) Tran, T. Q.; Park, S.; Weng, Z.; Lubomirsky, D. Plasma etching systems and methods with secondary plasma injection. KR 20170026216 A, 2019.

(7) Yasin, H.; Ahmed, W.; Ali, A.; Bhatti, A.; Rehman, N. Micro-plasma assisted synthesis of multifunctional D-fructose coated silver nanoparticles. *Mater. Res. Express* **2019**, *6*, 1050a1052.

(8) Khatoon, N.; Yasin, H.; Younus, M.; Ahmed, W.; Rehman, N.; Zakaullah, M.; Iqbal, M. Z. Synthesis and spectroscopic characterization of gold nanoparticles via plasma-liquid interaction technique. *AIP Adv.* **2018**, *8*, 015130.

(9) Wang, Y.; Liu, L.; Zhang, X.; Jiang, M.; Liu, C.; Zhang, Q. Plasma spatial distribution manipulation and electrical property enhancement through plasma coupling effect. *AIP Adv.* **2018**, *8*, 105313.

(10) Tariq, F.; Rehman, N.; Akhtar, N.; George, R. E.; Khan, Y.; Rahman, S. Room temperature photoluminescence in plasma treated rutile TiO2 (110) single crystals. *Vacuum* **2020**, *171*, 108999.

(11) Manakhov, A.; Kedroňová, E.; Medalová, J.; Černochová, P.; Obrusník, A.; Michlíček, M.; Shtansky, D. V.; Zajíčková, L. Carboxyl-anhydride and amine plasma coating of PCL nanofibers to improve their bioactivity. *Mater. Des.* **2017**, *132*, 257−265.

(12) Deehan, M.; Tsai, M. C.-H.; Lu, N.; Or, D. T.; Chang, M. Plasma cleaning apparatus and method. JP 2008029930 A, 2014.

(13) Peck, J. A.; Zonooz, P.; Curreli, D.; Panici, G. A.; Jurczyk, B. E.; Ruzic, D. N. High deposition rate nanocrystalline and amorphous silicon thin film production via surface wave plasma source. *Surf. Coat. Technol.* **2017**, *325*, 370−376.

(14) Heberlein, J.; Murphy, A. B. Thermal plasma waste treatment. *J. Phys. D: Appl. Phys.* **2008**, *41*, 053001.

(15) Foster, J. E. Plasma-based water purification: Challenges and prospects for the future. *Phys. Plasmas* **2017**, *24*, 055501.

(16) Lebouvier, A.; Iwarere, S. A.; d'Argenlieu, P.; Ramjugernath, D.; Fulcheri, L. Assessment of carbon dioxide dissociation as a new route for syngas production: a comparative review and potential of plasma-based technologies. *Energy Fuels* **2013**, *27*, 2712−2722.

(17) von Woedtke, T.; Haertel, B.; Weltmann, K.-D.; Lindequist, U. Plasma pharmacy−physical plasma in pharmaceutical applications. *Pharmazie-Int. J. Pharmaceut. Sci.* **2013**, *68*, 492−498.

(18) d'Agostino, R.; Favia, P.; Oehr, C.; Wertheimer, M. R. Low-temperature plasma processing of materials: Past, present, and future. *Plasma Processes Polym.* **2005**, *2*, 7−15.

(19) Moreau, M.; Orange, N.; Feuilloley, M. Non-thermal plasma technologies: new tools for bio-decontamination. *Biotechnol. Adv.* **2008**, *26*, 610−617.

(20) Nastuta, A. V.; Pohoata, V.; Topala, I. Atmospheric pressure plasma jet—Living tissue interface: Electrical, optical, and spectral characterization. *J. Appl. Phys.* **2013**, *113*, 183302.

(21) Busco, G.; Robert, E.; Chettouh-Hammas, N.; Pouvesle, J.-M.; Grillon, C. The emerging potential of cold atmospheric plasma in skin biology. *Free Radic. Biol. Med.* **2020**, *161*, 290−304.

(22) Daeschlein, G.; Napp, M.; Lutze, S.; Arnold, A.; von Podewils, S.; Guembel, D.; Jünger, M. Skin and wound decontamination of multidrug-resistant bacteria by cold atmospheric plasma coagulation. *JDDG J. der Deutschen Dermatol. Gesellschaft* **2015**, *13*, 143−149.

(23) Yan, D.; Cui, H.; Zhu, W.; Nourmohammadi, N.; Milberg, J.; Zhang, L. G.; Sherman, J. H.; Keidar, M. The specific vulnerabilities of cancer cells to the cold atmospheric plasma-stimulated solutions. *Sci. Rep.* **2017**, *7*, 1−12.

(24) Hoffmann, C.; Berganza, C.; Zhang, J. Cold Atmospheric Plasma: methods of production and application in dentistry and oncology. *Med. Gas Res.* **2013**, *3*, 21.

(25) Fridman, G.; Friedman, G.; Gutsol, A.; Shekhter, A. B.; Vasilets, V. N.; Fridman, A. Applied plasma medicine. *Plasma Process. Polym.* **2008**, *5*, 503−533.
(26) Morfill, G.; Shimizu, T.; Steffes, B.; Schmidt, H. Nosocomial infections—a new approach towards preventive medicine using plasmas. *New J. Phys.* **2009**, *11*, 115019.
(27) Stoffels, E.; Sakiyama, Y.; Graves, D. B. Cold atmospheric plasma: charged species and their interactions with cells and tissues. *IEEE Trans. Plasma Sci.* **2008**, *36*, 1441−1457.
(28) Heinlin, J.; Morfill, G.; Landthaler, M.; Stolz, W.; Isbary, G.; Zimmermann, J. L.; Shimizu, T.; Karrer, S. Plasma medicine: possible applications in dermatology. *JDDG J. der Deutschen Dermatol. Gesellschaft* **2010**, *8*, 968−976.
(29) Lu, X.; Bruggeman, P. J.; Reuter, S.; Naidis, G.; Bogaerts, A.; Laroussi, M.; Keidar, M.; Robert, E.; Pouvesle, J.-M.; Liu, D. Grand challenges in low temperature plasmas. *Front. Phys.* **2022**, 1036.
(30) Morabit, Y.; Hasan, M. I.; Whalley, R. D.; Robert, E.; Modic, M.; Walsh, J. L. A review of the gas and liquid phase interactions in low-temperature plasma jets used for biomedical applications. *Eur. Phys. J.* **2021**, *75*, 1−26.
(31) Rasouli, M.; Mehdian, H.; Hajisharifi, K.; Amini, E.; Ostrikov, K.; Robert, E. Plasma-activated medium induces apoptosis in chemotherapy-resistant ovarian cancer cells: High selectivity and synergy with carboplatin. *Plasma Processes Polym.* **2021**, *18*, 2100074.
(32) Maho, T.; Binois, R.; Brulé-Morabito, F.; Demasure, M.; Douat, C.; Dozias, S.; Bocanegra, P. E.; Goard, I.; Hocqueloux, L.; Le Helloco, C.; Orel, I.; Pouvesle, J.-M.; Prazuck, T.; Stancampiano, A.; Tocaben, C.; Robert, E. Anti-bacterial action of plasma multi-jets in the context of chronic wound healing. *J. Appl. Sci.* **2021**, *11*, 9598.
(33) Omran, A. V.; Busco, G.; Ridou, L.; Dozias, S.; Grillon, C.; Pouvesle, J.-M.; Robert, E. Cold atmospheric single plasma jet for RONS delivery on large biological surfaces. *Plasma Sources Sci. Technol.* **2020**, *29*, 105002.
(34) Morabit, Y.; Whalley, R. D.; Robert, E.; Hasan, M. I.; Walsh, J. L. Turbulence and entrainment in an atmospheric pressure dielectric barrier plasma jet. *Plasma Processes Polym.* **2020**, *17*, 1900217.
(35) Stancampiano, A.; Chung, T.-H.; Dozias, S.; Pouvesle, J.-M.; Mir, L. M.; Robert, E. Mimicking of human body electrical characteristic for easier translation of plasma biomedical studies to clinical applications. *IEEE Trans. Radiat. Plasma. Med. Sci.* **2019**, *4*, 335−342.
(36) Graves, D. B. The emerging role of reactive oxygen and nitrogen species in redox biology and some implications for plasma applications to medicine and biology. *J. Phys. D: Appl. Phys.* **2012**, *45*, 263001.
(37) Halliwell, B.; Gutteridge, J. M. *Free radicals in biology and medicine*; Oxford University Press: USA, 2015.
(38) Kim, J. Y.; Wei, Y.; Li, J.; Foy, P.; Hawkins, T.; Ballato, J.; Kim, S. O. Single-cell-level microplasma cancer therapy. *Small* **2011**, *7*, 2291−2295.
(39) Vijayarangan, V.; Delalande, A.; Dozias, S.; Pouvesle, J.-M.; Pichon, C.; Robert, E. Cold atmospheric plasma parameters investigation for efficient drug delivery in HeLa cells. *IEEE Trans. Radiat. Plasma Med. Sci.* **2017**, *2*, 109−115.
(40) Labay, F.; Roldán, C.; Tampieri, C.; Stancampiano, M.; Bocanegra, P. E.; Ginebra, M. P.; Canal, C. Enhanced generation of reactive species by cold plasma in gelatin solutions for selective cancer cell death. *ACS Appl. Mater. Interfaces* **2020**, *12*, 47256−47269.
(41) Lu, X.; Naidis, G. V.; Laroussi, M.; Reuter, S.; Graves, D. B.; Ostrikov, K. Reactive species in non-equilibrium atmospheric-pressure plasmas: Generation, transport, and biological effects. *Phys. Rep.* **2016**, *630*, 1−84.
(42) Vijayarangan, V.; Delalande, A.; Dozias, S.; Pouvesle, J.-M.; Robert, E.; Pichon, C. New insights on molecular internalization and drug delivery following plasma jet exposures. *Int. J. Pharm.* **2020**, *589*, 119874.
(43) Robert, E.; Darny, T.; Dozias, S.; Iseni, S.; Pouvesle, J.-M. New insights on the propagation of pulsed atmospheric plasma streams: From single jet to multi jet arrays. *Phys. Plasma.* **2015**, *22*, 122007.
(44) Obradović, B.; Ivković, S.; Kuraica, M. Spectroscopic measurement of electric field in dielectric barrier discharge in helium. *Appl. Phys. Lett.* **2008**, *92*, 191501.
(45) Chung, T.-H.; Stancampiano, A.; Sklias, K.; Gazeli, K.; André, F. M.; Dozias, S.; Douat, C.; Pouvesle, J.-M.; Santos Sousa, J.; Robert, É.; Mir, L. Cell electropermeabilisation enhancement by non-thermal-plasma-treated pbs. *Cancers* **2020**, *12*, 219.
(46) Zhang, Q.; Zhuang, J.; von Woedtke, T.; Kolb, J. F.; Zhang, J.; Fang, J.; Weltmann, K.-D. Synergistic antibacterial effects of treatments with low temperature plasma jet and pulsed electric fields. *Appl. Phys. Lett.* **2014**, *105*, 104103.
(47) Bekeschus, S.; Favia, P.; Robert, E.; von Woedtke, T. White paper on plasma for medicine and hygiene: Future in plasma health sciences. *Plasma Processes Polym.* **2019**, *16*, 1800033.
(48) Deepak, G. D. Review on recent advances in cold plasma technology. *Eur. Phys. J. Appl. Phys.* **2022**, *97*, 39.
(49) Khan, M.; Rehman, N.; Khan, S.; Ullah, N.; Masood, A.; Ullah, A. Spectroscopic study of CO2 and CO2−N2 mixture plasma using dielectric barrier discharge. *AIP Adv.* **2019**, *9*, 085015.
(50) Rahman, S. u.; Ahmed, W.; Rehman, N. U.; Alkhedher, M.; Tag El Din, E. M. Fabrication of Graphene Sheets Using an Atmospheric Pressure Thermal Plasma Jet System. *Energies* **2022**, *15*, 7245.
(51) Farooq, M.; Khan, M. I.; Rehman, N. Spectrochemical Analysis of Ozone Density for Pulsed Plasma Discharge in Oxygen−Water Mixture. *Plasma Chem. Plasma Process.* **2022**, 1−16.
(52) Turan, N.; Saeidi-Javash, M.; Chen, J.; Zeng, M.; Zhang, Y.; Go, D. B. Atmospheric Pressure and Ambient Temperature Plasma Jet Sintering of Aerosol Jet Printed Silver Nanoparticles. *ACS Appl. Mater. Interfaces* **2021**, *13*, 47244−47251.
(53) Ghimire, B.; Szili, E. J.; Patenall, B. L.; Lamichhane, P.; Gaur, N.; Robson, A. J.; Trivedi, D.; Thet, N. T.; Jenkins, A. T. A.; Choi, E. H.; Short, R. D. Enhancement of hydrogen peroxide production from an atmospheric pressure argon plasma jet and implications to the antibacterial activity of plasma activated water. *Plasma Sources Sci.* **2021**, *30*, 035009.
(54) Iza, F.; Kim, G. J.; Lee, S. M.; Lee, J. K.; Walsh, J. L.; Zhang, Y. T.; Kong, M. G. Microplasmas: sources, particle kinetics, and biomedical applications. *Plasma Process.* **2008**, *5*, 322−344.
(55) von Woedtke, T.; Metelmann, H. R.; Weltmann, K. D. Clinical plasma medicine: state and perspectives of in vivo application of cold atmospheric plasma. *Contrib. Plasma Phys.* **2014**, *54*, 104−117.
(56) Harper, J. D.; Charipar, N. A.; Mulligan, C. C.; Zhang, X.; Cooks, R. G.; Ouyang, Z. Low-temperature plasma probe for ambient desorption ionization. *Anal. Chem.* **2008**, *80*, 9097−9104.
(57) Kim, S. J.; Chung, T. Cold atmospheric plasma jet-generated RONS and their selective effects on normal and carcinoma cells. *Sci. Rep.* **2016**, *6*, 1−14.
(58) Saadati, F.; Mahdikia, H.; Abbaszadeh, H.-A.; Abdollahifar, M.-A.; Khoramgah, M. S.; Shokri, B. Comparison of Direct and Indirect cold atmospheric-pressure plasma methods in the B16F10 melanoma cancer cells treatment. *Sci. Rep.* **2018**, *8*, 7689.
(59) Townshend, A. *RWB Pearse and AG Gaydon, The Identification of Molecular Spectra: Chapman and Hall, London, 4th edn., 1976, viii+ 407 pp., price£ 20.00*; Elsevier, 1977.
(60) Khan, M. I.; Khan, M. A.; Zaman, M. I.; ur Rehman, N.; Masood, A.; Ullah, N. Enhancement of O-atom density through collisions with Ne by laser-produced plasma in Ne−O2 gas mixtures and possible energy transfer mechanism. *Int. J. Mod. Phys. B* **2019**, *33*, 1950198.
(61) Khan, M. A.; Al-Jalal, A. M. Dissociation of O 2 in low pressure glow discharges in He−O 2, Ne−O 2, and Ar−O 2 gas mixtures. *J. Appl. Phys.* **2008**, *104*, 123302.
(62) Popa, S. Influence of pressure on spectral intensities in a flowing nitrogen glow discharge. *J. Phys. D: Appl. Phys.* **1996**, *29*, 416.
(63) Barkhordari, A.; Ganjovi, A. Technical characteristics of a DC plasma jet with Ar/N2 and O2/N2 gaseous mixtures. *Chin. J. Phys.* **2019**, *57*, 465−478.
(64) Graves, D. B. The emerging role of reactive oxygen and nitrogen species in redox biology and some implications for plasma

https://doi.org/10.1021/acsomega.2c07810
ACS Omega 2023, 8, 12028−12038

applications to medicine and biology. *J. Phys. D: Appl. Phys.* **2012**, *45*, 263001.
(65) Khan, F.; Rehman, N.; Naseer, S.; Naveed, M.; Qayyum, A.; Khattak, N.; Zakaullah, M. Diagnostic of 13.56 MHz RF sustained Ar−N2 plasma by optical emission spectroscopy. *Eur. Phys. J. Appl. Phys.* **2009**, *45*. DOI: 10.1051/epjap:2008198
(66) Anjum, Z.; Younus, M.; Rehman, N. Evolution of plasma parameters in capacitively coupled He−O2/Ar mixture plasma generated at low pressure using 13.56 MHz generator. *Phys. Scr.* **2020**, *95*, 045403.
(67) *NIST Atomic Spectra Database*, version 5.9; NIST, 2021. https://physics.nist.gov/asd.
(68) Chung, T.; Ra Kang, H.; Bae, M. K. Optical emission diagnostics with electric probe measurements of inductively coupled Ar/O2/Ar-O2 plasmas. *Phys. Plasmas* **2012**, *19*, 113502.
(69) Qayyum, A.; Zeb, S.; Naveed, M.; Rehman, N.; Ghauri, S.; Zakaullah, M. Optical emission spectroscopy of Ar−N2 mixture plasma. *J. Quant. Spectrosc. Radiat. Transfer* **2007**, *107*, 361.
(70) Bourdon, A.; Darny, T.; Pechereau, F.; Pouvesle, J.-M.; Viegas, P.; Iséni, S.; Robert, E. Numerical and experimental study of the dynamics of a μs helium plasma gun discharge with various amounts of N2 admixture. *Plasma Sources Sci. Technol.* **2016**, *25*, 035002.
(71) Lu, X.; Naidis, G.; Laroussi, M. a.; Ostrikov, K. Guided ionization waves: Theory and experiments. *Phys. Rep.* **2014**, *540*, 123−166.
(72) Xiong, Z.; Robert, E.; Sarron, V.; Pouvesle, J.-M.; Kushner, M. J. Atmospheric-pressure plasma transfer across dielectric channels and tubes. *J. Phys. D: Appl. Phys.* **2013**, *46*, 155203.
(73) Lu, X.; Laroussi, M.; Puech, V. On atmospheric-pressure non-equilibrium plasma jets and plasma bullets. *Plasma Sources Sci. Technol.* **2012**, *21*, 034005.
(74) Robert, E.; Sarron, V.; Riès, D.; Dozias, S.; Vandamme, M.; Pouvesle, J. M. Characterization of pulsed atmospheric-pressure plasma streams (PAPS) generated by a plasma gun. *Plasma Sources Sci. Technol.* **2012**, *21*, 034017.
(75) Darny, T.; Pouvesle, J. M.; Puech, V.; Douat, C.; Dozias, S.; Robert, E. Analysis of conductive target influence in plasma jet experiments through helium metastable and electric field measurements. *Plasma Sources Sci. Technol.* **2017**, *26*, 045008.
(76) Farooq, M.; Ijaz, U.; Anjum, Z.; Rehman, N. U. Nanosecond Pulsed Plasma Discharge in Oxygen−Water Mixture: Effect of Discharge Parameters on Pre-and Post-Breakdown Characteristics. *IEEE Trans. Plasma Sci.* **2022**, *50*, 942−953.
(77) Konjević, N.; Lesage, A.; Fuhr, J. R.; Wiese, W. L. Experimental Stark widths and shifts for spectral lines of neutral and ionized atoms (a critical review of selected data for the period 1989 through 2000). *J. Phys. Chem. Ref. Data* **2002**, *31*, 819−927.
(78) Dong, L.; Ran, J.; Mao, Z. Direct measurement of electron density in microdischarge at atmospheric pressure by Stark broadening. *Appl. Phys. Lett.* **2005**, *86*, 161501.
(79) Hu, S.; Xia, X.; Gai, B.; Liu, D.; Cai, X.; Lou, M.; Li, X.; Guo, J. Laser-induced multiphoton and collisional ionizations in sodium-argon mixture. *J. Lumin.* **2020**, *225*, 117370.
(80) Vasiljević, M. M.; Spasojević, D.; Šišović, N. M.; Konjević, N. Stark effect of Ar I lines for electric field strength diagnostics in the cathode sheath of glow discharge. *Europhys. Lett.* **2017**, *119*, 55001.

https://doi.org/10.1021/acsomega.2c07810
ACS Omega 2023, 8, 12028−12038